Anharmonic vibrational spectroscopy of germanium-containing clusters, Ge_xC_{4-x} and Ge_xSi_{4-x} (x = 0-4), for interstellar detection

A. Mackenzie Flowers, Alex Brown,* and Mariusz Klobukowski*

Department of Chemistry, University of Alberta, Edmonton, AB T6G 2G2, Canada

E-mail: alex.brown@ualberta.ca; mariusz@ualberta.ca

Abstract

An extensive, high-level theoretical study on tetra-atomic germanium carbide/silicide clusters is presented. Accurate harmonic and anharmonic vibrational frequencies and rotational constants are calculated at the CCSD(T)-F12a(b)/cc-pVT(Q)Z-F12 levels of theory. With growing capabilities to discern more of the chemical composition of the interstellar medium (ISM), an accurate database of reference material is required. The presence of carbon is ubiquitous in the ISM, and silicon is known to be present in interstellar dust grains, however germanium-containing molecules remain elusive. To begin understanding the presence and role of germanium in the ISM, we present this study of the vibrational and rotational spectroscopic properties of various germanium-containing molecules to aid in their potential identification in the ISM with modern observational tools such as the James Webb Space Telescope. Structures studied herein include rhomboidal (r-), diamond (d-), and trapezoidal (t-) tetra-atomic molecules of the form Ge_xC_{4-x} and Ge_xSi_{4-x}, where x=0-4. The most promising structure for detection is r-Ge_2C_2 via the ν_4 mode with a frequency of 802.7 cm^{-1} (12.5 μm) and an intensity of 307.2 km mol^{-1}. Other molecules potentially detectable, i.e., through

vibrational modes or rotational transitions, include r-Ge_3C, r-$GeSi_3$, d-GeC_3, r-GeC_3, and t-Ge_2C_2.

Introduction

With the launch of the James Webb Space Telescope (JWST) in 2021, the ability to peer into the universe and pull out information from it has vastly improved. The instrumentation on JWST provides data in the mid-IR range (0.6 - 28.3 μm [$\sim$353 - $\sim$16667 cm^{-1}]) at a higher sensitivity, drastically increasing the possibility of identifying new compounds through infrared spectroscopy. For some of the more exotic and elusive molecules that might exist in the interstellar medium (ISM), high-level computational studies are an important step in potential identification of molecules in space. Accurate theoretical data provide reference points for collected astronomical observations. To that end, specifically with JWST's operations in the mid-IR range, accurate ro-vibrational data are needed to provide reference for the spectra that are measured.

An area of interest to astrochemists and astronomers is the study of star-forming regions and protoplanetary disk formation,[1,2] including the formation of dust grains in the ISM. Determining the composition of these dust grains and observing their accretion into protoplanetary disks could help elucidate what kind of stars and planetesimals might be forming in different regions of space.

Silicon carbide clusters have been suggested to be involved in the formation of SiC dust grains in the ISM, which have been seen in proto-planetary dust clouds.[3–7] These clusters are thought to be formed from the result of carbon and silicon formation through nucleosynthesis in asymptotic giant branch (AGB) stars.[6,8] However, their fellow group member germanium is also known to form through nucleosynthesis in AGB stars through the slow neutron capture s-process.[9,10]

Throughout the ISM, germanium is much less abundant than carbon and silicon and

might prove more elusive to detect. As a result, interstellar germanium chemistry is less documented. Germanium has been detected both near and far: in the atmosphere of Jupiter, planetary nebulae, and in some of the most distant galaxies.[9,11,12] Understanding the pathways germanium takes to be dispersed throughout the universe is an interesting topic that could give more insight into dust grain formation and rocky planet formation from resulting dust clouds. With the recent discovery of an iron-rich sub-earth exoplanet, GJ 367b, orbiting a nearby dwarf star, there is no end to the interesting exoplanets that could be found.[13] With the potential to discover more metal-rich planets, it's important to shed light on the chemistry of heavier elements throughout the ISM.

To begin understanding the chemistry of interstellar germanium, there is a need for determining structures and corresponding spectroscopic signatures for model molecules. Currently, a small group of silicon carbide molecules including the diatomic SiC, triatomic species SiC_2 and Si_2C, as well as the cyclic tetra-atomic SiC_3 has been identified in the ISM.[3,5,7,14,15] With the potential for various permutations of tetra-atomic germanium silicide and carbide analogues of SiC tetra-atomics, we can consider these tetra-atomics as a starting point of interest.

Multiple experimental and computational studies have been previously carried out on silicon carbide tetra-atomic clusters,[14,16–27] but only a few have investigated germanium carbide and silicide clusters.[28,29] The smaller germanium carbide and germanium silicide (triatomic) molecules as well as linear molecules have been previously studied both experimentally and computationally at various levels of theory.[28–34] However, in the area of germanium tetra-atomics, an extensive study of the various permutations of tetra-atomic germanium carbide and silicide clusters has not yet been done, computationally or experimentally. Also, more accurate computational methods have become accessible since previous publications and the determination of results at a higher-level of theory is worthwhile for use in astrochemical pursuits.

As mentioned, in the context of interstellar dust grains, tetra-atomic silicon carbide clus-

ters (TASCCs) have recently been extensively studied by Sehring et al. using the CCSD(T)-F12b method with basis sets cc-pVTZ-F12 and cc-pCVTZ-F12.[16] The second method employs the cc-pCVTZ-F12 basis set to incorporate core electron correlation and scalar relativity effects.[35,36] Herein, we study tetra-atomic germanium carbide and silicide clusters at a similar level of theory. All structures studied consist of a quadrilateral motif with a transannular bond that include molecules of the form Ge_xZ_{4-x} (x=0-4), where Z is either carbon or silicon.

Both pure carbon and silicon tetra-atomic clusters have been previously studied at the coupled-cluster level of theory including CCSD(T)/cc-pCV5Z[37] and CCSD(T)-F12b/cc-p(C)VTZ-F12 respectively,[16] and the pure carbon cluster has also been studied experimentally.[38,39] Therefore quite accurate spectral data are already present for them. However, for completeness we have included them in our current study.

Moving to the first of the sets of germanium analogues, GeC_3 and $GeSi_3$, both have been looked at previously computationally, however only GeC_3 has had (harmonic) vibrational data generated.[28] For the cyclic GeZ_3 structures, there exist two isomers: diamond GeZ_3 and rhomboidal GeZ_3, which will be from here on be referred to as d-GeZ_3 and r-GeZ_3, respectively. The d-GeZ_3 is identified by the transannular Z-Z bond and the r-GeZ_3 by a Ge-Z transannular bond. All four of these structures exhibit C_{2v} symmetry. In the case of both r- and d-GeC_3, the available theoretical data was obtained using density functional theory (DFT) with the B3LYP functional,[40,41] CCSD,[42] and second-order Møller-Plesset perturbation theory (MP2), all in conjunction with the aug-cc-pVTZ basis set.[28]

With the Ge_2Z_2 structures, there are three isomers to consider: d- and r- as well as a trapezoidal shaped (t-) isomer. For these structures, the d- isomers are identified by a transannular Ge-Ge bond, the t- isomers by a transannular Ge-Z bond, and the r- isomers by a transannular Z-Z bond. Both r- isomers and the d-Ge_2Si_2 isomer exhibit D_{2h} symmetry. The two t-Ge_2Z_2 structures exhibit C_s symmetry. Finding an optimized structure for the remaining d-Ge_2C_2 isomer proved challenging and this will be discussed further below.

However, we predict it to exist in either a planar or a boat-like configuration, both with C_{2v} symmetry. Similarly to the r- and d- structures of GeC_3, previous theoretical data for the r- and t-Ge_2Z_2 structures are available.[28]

Lastly, there are four Ge_3Z structures of interest, with d- and r- isomers as in the GeZ_3 structures. The r- isomers are again distinguished by a Ge-Z transannular bond and the d- isomers by a Ge-Ge transannular bond. The d-Ge_3C has C_s symmetry, having a slight dihedral angle taking it out of plane and out of C_{2v} symmetry, which is seen in the three other structures in this group (r-Ge_3C, d-Ge_3Si, r-Ge_3Si). Of these four structures, only d-Ge_3C has been studied previously at the B3LYP/6-311G(3df) level of theory.[30]

It is worth noting that while both carbon and silicon have one naturally occurring isotope dominating in abundance (>90%), germanium has multiple isotopes with relatively high abundances, specifically ^{74}Ge, ^{72}Ge, and ^{70}Ge, with abundances of 36.5%, 27.4%, and 20.5%, respectively.[43] Other naturally occuring isotopes with smallar abundances are ^{73}Ge and ^{76}Ge, with abundances of 7.76% and 7.75%, respectively.[43] The effect of these isotopes on detectable spectra will be discussed further below. For the purpose of this study, we have used the most abundant isotope masses for each atom (^{12}C, ^{28}Si, and ^{74}Ge).

As many of these structures have not yet been examined computationally, and those that have been studied have not had high-level methods applied to them, there exists an opening to apply modern wavefunction-based approaches to the study of these tetra-atomic germanium-contatining structures and their corresponding ro-vibrational spectra. Herein, we present theoretical spectroscopic data for structures described above using high-level computational methods. Accurate (harmonic and anharmonic) vibrational frequencies and (vibrationally-averaged) rotational constants could help in identifying these structures in planetary atmospheres, planetary nebulae, near distant AGB stars, and other ISM environments through use of JWST.

Computational Methods

All computations were carried out as follows. Geometries, harmonic, and anharmonic vibrational frequencies were determined using the explicitly-correlated coupled-cluster theory at the singles, doubles, and perturbative triples level CCSD(T)-F12;[44–46] depending on the basis set size, either the F12a or F12b formalism was used.[45] The cc-pVXZ-F12 basis sets were used for carbon and silicon atoms, while a pseudopotential with associated basis set (cc-pVXZ-PP-F12) was used for germanium atoms, where X=T or Q.[47,48] It has been previously shown that the F12a method provides a better estimate of correlation energies for smaller basis sets (double-/triple-zeta), while the F12b method is reportedly better when using larger basis sets (quadruple-zeta); both methods converge to the complete basis set (CBS) limit from above and below, respectively.[45,49] The names of the two methods will be herein shortened as "F12a/TZ" and "F12b/QZ."

The MOLPRO 2023.2 software was used for all calculations in this work.[50–52] For each molecule, geometry optimization was first carried out at the F12a/TZ or F12b/QZ level of theory followed by harmonic frequency calculations.[53–56] Default convergence criteria were used for all optimization calculations. Dipole moments were retrieved at all optimized geometries. Subsequently, anharmonic frequencies were calculated through second-order vibrational perturbation theory (VPT2) as implemented in MOLPRO.[57–59] An analytical representation of the potential energy surface is generated in the form of a quartic force field, which is then used to retrieve force constants. Using VPT2, anharmonic vibrational frequencies and vibrationally-averaged rotational constants were obtained. As the F12a/TZ and F12b/QZ methods are both able to converge to the complete basis set limit,[45,46] F12b/QZ was only applied to a select few systems for comparison with F12a/TZ and determination of the cost/accuracy benefit.

Results and Discussion

Using the methods outlined above, computations were performed on the suite of germanium carbide and germanium silicide molecules of the form Ge_xZ_{4-x}, where x = 0-4. Across all species, the frequencies of the calculated anharmonic vibrational modes mostly fall within the 0.6 - 28.3 μm ($\sim$353 - $\sim$16667 cm^{-1}) mid-IR range of JWST.

As mentioned previously, many of these molecules have not yet been studied experimentally or theoretically. However, there exist previous studies on a few structures investigated herein, which have been used for comparison with the present work.[16,28] Equilibrium structures of all systems studied are presented in figures with bond distances and angles shown, while Cartesian coordinates and energies for the optimized structures are found in the Supporting Information.

Table 1 shows relative electronic energies as well as those corrected for harmonic and anharmonic zero-point vibrational energies (ZPVE) of optimized structures (in kJ mol^{-1}), with respect to the lowest lying isomer in each group, as well as symmetry of each structure and dipole moments. The zero-point energies as well as the energies of each structure with the ZPVE added and their relative energies are shown in Table S1.

r-Z_4

The equilibrium structures of the mono-elemental tetra-atomic clusters, C_4, Si_4, and Ge_4 are shown in Figure 1. Vibrational frequencies for r-Si_4 and r-Ge_4 are shown in Table 2, while their rotational constants can be found in Table S2. As the tetra-atomic carbon cluster has been studied extensively, only Si_4 and Ge_4 results are shown here; those for carbon can be found in Tables S3 and S4. Anharmonic vibrational frequencies for r-C_4 were calculated at both the F12a/TZ and F12b/QZ levels of theory. To compare different methods, the mean absolute percent deviation (MAPD), defined as the absolute difference between results obtained with the two methods divided by the "more accurate" method divided by the

Table 1: Ge_xZ_y family relative energies (in kJ mol^{-1}) of optimized geometries with inclusion of harmonic and anharmonic zero-point vibrational energy (ZPVE). Relative energies are taken with respect to the lowest energy isomer in each group. Dipole moments (μ, in Debye) at each optimized geometry are included. All results at F12a/TZ level of theory.

Structure	Symmetry	ΔE_0^{ZPVE}		μ
		(Harmonic)	(Anharmonic)	
d-GeC_3	C_{2v}	0.000	0.000	5.40
r-GeC_3	C_{2v}	10.540	10.603	2.95
t-Ge_2C_2	C_s	0.000	0.000	3.52
r-Ge_2C_2	D_{2h}	20.413	20.381	0.00
d-Ge_2C_2[a]	C_{2v}	397.491		2.03
r-Ge_3C	C_{2v}	0.000	0.000	0.11
d-Ge_3C	C_s	189.830	189.778	0.98
d-$GeSi_3$	C_{2v}	0.000	0.000	0.79
r-$GeSi_3$	C_{2v}	16.982	16.957	0.01
r-Ge_2Si_2	D_{2h}	0.000	0.000	0.00
t-Ge_2Si_2	C_s	12.871	12.862	0.77
d-Ge_2Si_2	D_{2h}	32.643	32.637	0.00
r-Ge_3Si	C_{2v}	0.000	0.000	0.04
d-Ge_3Si	C_{2v}	15.666	15.660	0.76

[a]CCSD(T)-F12a/cc-pVDZ-F12

number of cases multipled by 100%, is reported where relevant, i.e.

$$MAPD = \left(\frac{1}{N} \sum_{i=1}^{N} \left| \frac{A_i - A_{ref}}{A_{ref}} \right| \right) \times 100\%$$

.

For r-C_4 the F12a/TZ method is seen to have a MAPD of 0.12% from the F12b/QZ results, but with the computation taking around nine times less wall clock time to complete. This comparison supports the previous observation[45,46] that the two methods converge to similar results. For r-Si_4, computed results are similar to those computed at the best current level of theory in the literature from Sehring et al.[16] Computed anharmonic vibrational frequencies and rotational constants show MAPDs (for F12a/TZ with respect to F12-TZ-cCR) of 0.60% and 1.31% respectively, indicating the F12a/TZ method has exceptionally high accuracy in comparison with the F12-TZ-cCR method used in the work of Sehring et al.[16] This comparison demonstrates the small but non-negligible effects of core-valence correlation and relativistic effects that are accounted for in the F12-TZ-cCR approach.[16]

For the tetra-atomic pure germanium structure, the vibrational mode most promising for observation would be ν_6 with an intensity of 58.8 km mol^{-1}, however its frequency of 280.0 cm^{-1} falls outside the range of JWST's mid-IR observing capabilities. With no permanent dipole moment, this molecule is unlikely to be detected with current instruments whether through IR spectroscopy or rotational spectroscopy.

GeZ_3

Optimized geometries for each GeZ_3 structure are shown in Figure 2. Between the two GeC_3 structures, d-GeC_3 was found to lie 1.140 kJ mol^{-1} lower (0.776 kJ mol^{-1} when corrected for ZPVE) than r-GeC_3. Although the former is found to be the lowest energy structure, the energy difference between the two might point towards a very small barrier for interconversion.

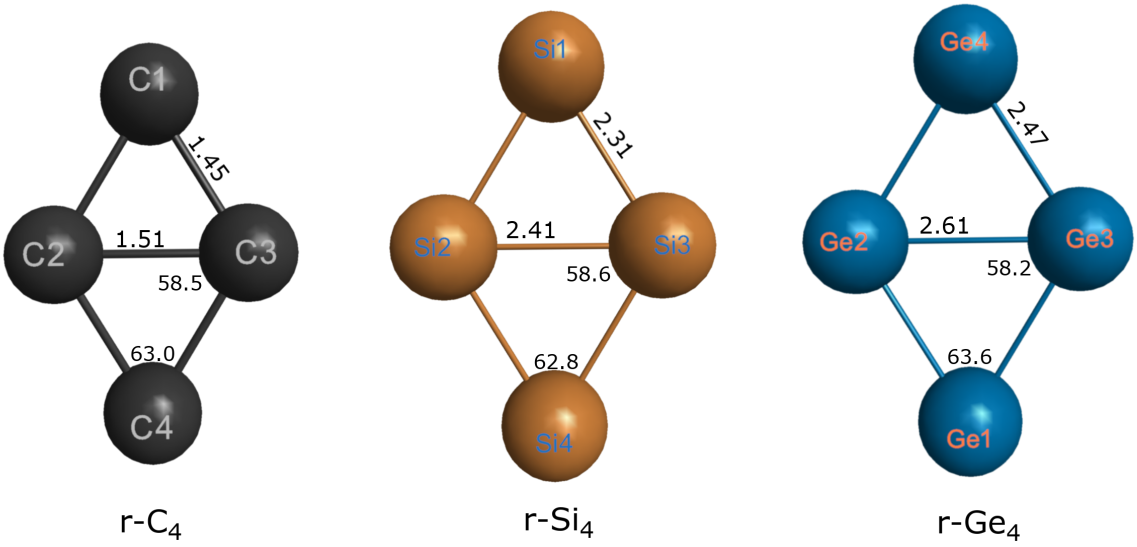

Figure 1: Optimized geometries of Z_4 structures at the CCSD(T)-F12a/cc-pVTZ-F12 level of theory. Bond lengths shown in Å, angles in degrees.

Table 2: Harmonic and anharmonic fundamental vibrational frequencies (in cm^{-1}) of r-Si_4 and r-Ge_4. MAPD is shown for F12a/TZ with respect to F12-TZ-cCR for anharmonic frequencies. Intensities (in km mol^{-1}) for F12a/TZ calculations are from this work.

Mode	Symmetry	Harmonic		Anharmonic		Intensity
r-Si_4	D_{2h}	F12a/TZ	F12-TZ-cCR[a]	F12a/TZ	F12-TZ-cCR[a]	
6	B_{1u}	510.4	512.5	503.3	505.9	147.1
5	A_g	476.9	479.2	471.7	476.1	0.0
4	B_{2g}	439.4	442.4	433.3	436.6	0.0
3	A_g	350.4	353.0	347.5	350.0	0.0
2	B_{3u}	253.0	254.0	250.5	251.9	8.3
1	B_{2u}	75.4	75.1	76.3	76.2	2.2
MAPD				0.60		
r-Ge_4	D_{2h}					
6	B_{1u}	282.8		280.0		58.8
5	A_g	265.4		266.6		0.0
4	B_{2g}	239.5		237.1		0.0
3	A_g	188.1		187.0		0.0
2	B_{3u}	133.1		132.0		0.1
1	B_{2u}	49.1		49.4		0.2

[a]Sehring et al. 2022

Similarly, d-$GeSi_3$ was found to be the lower energy isomer compared to r-$GeSi_3$, with an energy difference of only 17.256 kJ mol^{-1}. Considering the very small energy gaps between the isomers, it is worthwhile exploring the conversion between them and determining transition states between the isomers. Previously, d-SiC_3 was detected in space towards IRC+10216 through its rotational spectrum by the ALMA telescope array.[14] When considering similarities between d-SiC_3 and d-GeC_3, they both have large dipole moments of 4.2 and 5.4 D, respectively.[16] Although d-GeC_3 does not have the most intense of vibrational modes between the GeC_3 isomers, its large dipole moment indicates the possibility of detection by rotational spectroscopy.

Vibrational frequencies and rotational constants for the GeZ_3 structures are presented in Tables 3-5. All four structures have one vibrational mode with relatively strong intensity, with the r- isomers having the strongest at 112.0 and 107.0 km mol^{-1} for GeC_3 and $GeSi_3$, respectively. These two vibrational modes correspond to the 2-3-4 asymmetric stretch where atoms 2, 3, and 4 are either carbon or silicon as seen in Figure 2. Many vibrational modes fall within the observable range of JWST, however the smaller frequency modes (<353 cm^{-1}, about half of them for the $GeSi_3$ isomers), fall outside of that range.

Computed anharmonic vibrational frequencies for d-GeC_3 at the F12a/TZ level have a MAPD of 0.12% relative to the F12b/QZ frequencies. However, the computation time increased by almost a factor of six for the F12b/QZ calculation compared to the F12a/TZ calculation. Therefore, when considering the method of choice for these systems, the increase in computational cost associated with F12b/QZ is likely not worth the small gain in accuracy.

Ge_2Z_2

Six Ge_2Z_2 structures were considered. Equilibrium structures for the three Ge_2C_2 and three Ge_2Si_2 isomers are shown in Figure 3. Vibrational frequencies and rotational constants for each structure are presented in Tables 6 and 7. For this group of structures we have again chosen to use both F12a/TZ and F12b/QZ to compare results for r-Ge_2C_2. Frequencies and

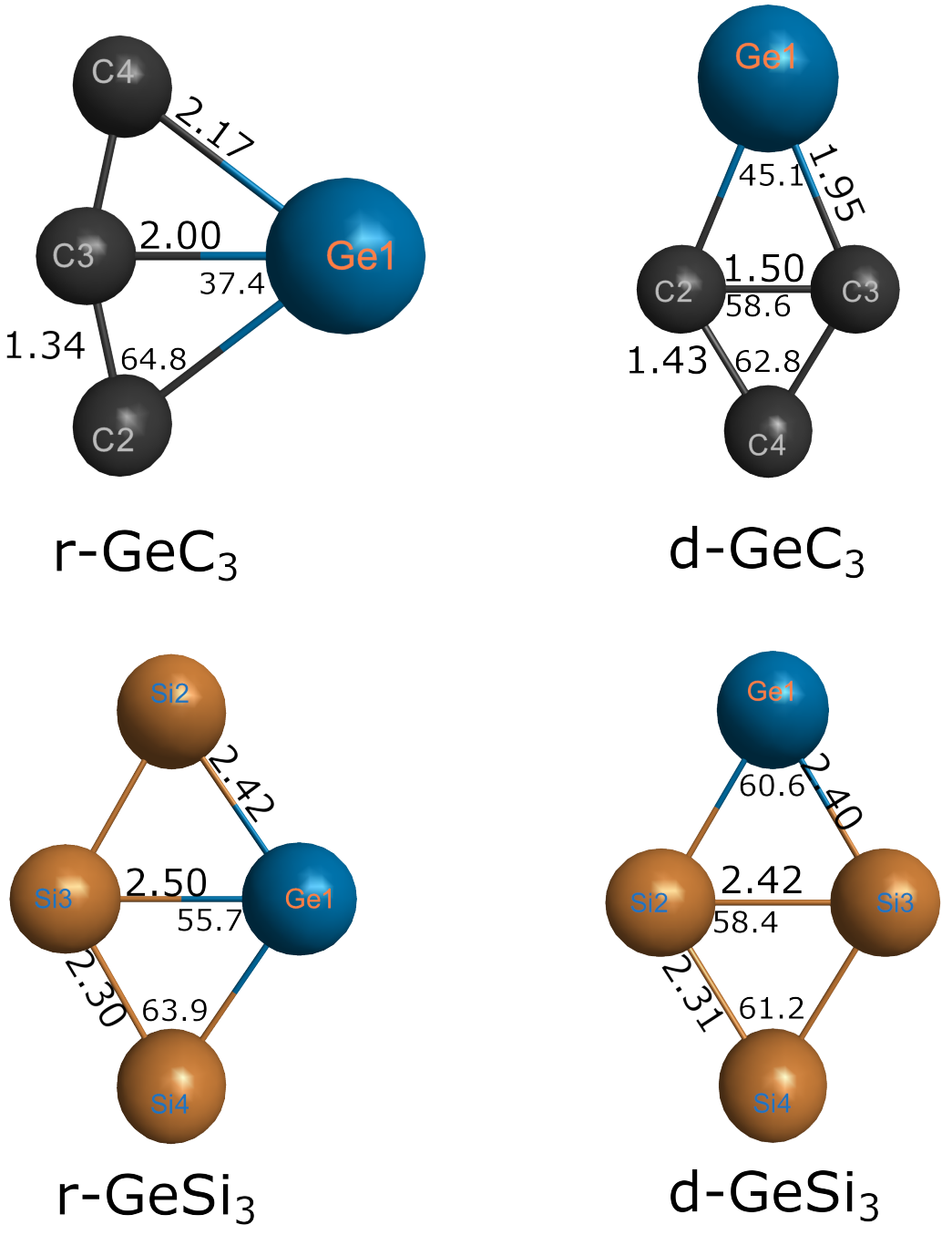

Figure 2: Optimized geometries of GeZ_3 structures at the CCSD(T)-F12a/cc-pVTZ-F12 level of theory. Bond lengths shown in Å, angles in degrees.

Table 3: Harmonic and anharmonic fundamental vibrational frequencies (in cm^{-1}) of GeC_3 isomers. Both F12a/TZ and F12b/QZ have been used for d-GeC_3. MAPD is shown for F12a/TZ with respect to F12b/QZ for anharmonic frequencies. Intensities in km mol^{-1}.

Mode	Symmetry	Harmonic		Anharmonic		Intensity
d-GeC_3		a/TZ	b/QZ	a/TZ	b/QZ	
6	A_1	1389.7	1390.6	1421.8	1422.8	88.9
5	B_1	1020.6	1021.3	993.0	993.6	1.4
4	A_1	912.2	912.4	891.9	892.2	50.6
3	A_1	518.5	519.0	512.7	513.3	72.8
2	B_1	355.4	356.3	348.1	349.0	36.9
1	B_2	219.9	220.0	219.9	220.3	3.5
MAPD				0.12		
r-GeC_3						
6	B_2	1574.4		1538.3		112.0
5	A_1	1118.0		1096.3		2.2
4	A_1	720.4		709.8		28.1
3	A_1	415.1		408.8		26.9
2	B_2	338.1		332.4		2.4
1	B_1	178.3		191.8		24.6

[a]F12a/TZ intensities

Table 4: Harmonic and anharmonic fundamental vibrational frequencies (in cm^{-1}) of $GeSi_3$ isomers using F12a/TZ. Intensities in km mol^{-1}.

Mode	Symmetry	Harmonic	Anharmonic	Intensity
d-$GeSi_3$				
6	A_1	496.4	490.0	92.1
5	A_1	426.2	421.9	29.2
4	B_1	416.7	411.1	0.1
3	A_1	273.5	271.7	7.9
2	B_1	217.8	216.4	5.5
1	B_2	69.0	69.7	1.1
r-$GeSi_3$				
6	B_2	503.3	495.8	107.0
5	A_1	430.2	430.0	1.5
4	B_2	326.5	322.6	13.9
3	A_1	308.1	305.8	1.9
2	A_1	209.2	207.5	1.1
1	B_1	72.9	73.1	2.0

Table 5: Equilibrium (e) and vibrationally-averaged (0) rotational constants of GeC_3 and $GeSi_3$ isomers in MHz at the F12a/TZ level of theory and F12b/QZ for d-GeC_3. In each case, ν_6 was the most intense mode, thus vibrationally-averaged constants for this mode are included (6).

Constant	d-GeC_3	F12b/QZ	Constant	r-GeC_3	Constant	d-$GeSi_3$	Constant	r-$GeSi_3$
A_e	37654.4	37685.7	A_e	12195.1	A_e	6175.1	A_e	3530.6
B_e	3891.2	3893.8	B_e	6286.6	B_e	1387.7	B_e	2264.8
C_e	3526.7	3529.1	C_e	4148.2	C_e	1133.1	C_e	1379.7
A_0	37333.8	37364.3	A_0	12929.4	A_0	6150.5	A_0	3520.1
B_0	3876.4	3879.0	B_0	6252.5	B_0	1385.3	B_0	2260.3
C_0	3509.5	3511.9	C_0	4128.7	C_0	1130.5	C_0	1376.1
A_6	36031.0	36065.6	A_6	12287.4	A_6	6096.4	A_6	3500.4
B_6	3885.1	3887.6	B_6	6223.3	B_6	1388.6	B_6	2264.3
C_6	3521.0	3523.4	C_6	4142.8	C_6	1134.0	C_6	1379.0
MAPD	0.08							

rotational constants for the two methods show MAPDs of 0.18% and 0.07%, respectively, for F12a/TZ with respect to F12b/QZ, again supporting the conclusion that the increase in computational cost (a factor of eight in this case) has a negligible effect on accuracy gained. Among all structures studied in this work, r-Ge_2C_2 showed a vibrational frequency with an intensity well above all other vibrational modes. An intensity of 307.2 km mol^{-1} is predicted for ν_3 which is the Ge(1)-C(1) and Ge(2)-C(2) symmetric stretch at 801.7 cm^{-1}. With such a large intensity, observation of this mode is a likely candidate for detection by JWST. The t-isomer does not have any vibrational modes with high intensities, and is thus less likely to be detected by JWST.

As mentioned, the d-Ge_2C_2 structure posed a challenge to optimize. An equilibrium structure was found using the smaller double-zeta basis set (cc-pVDZ-F12),[47] with a boat-like geometry. However, this structure was found to have a T1 diagnostic[60] of 0.098, suggesting multi-reference character, and thus this level of theory might not allow for an accurate description of this structure. A table of T_1 diagnostics for all clusters considered in this work is shown in Table S5. For the majority of structures, T_1 was below the 0.02 threshold indicating single-reference character. The d-Ge_3C has a T_1 value of 0.039, which indicates that

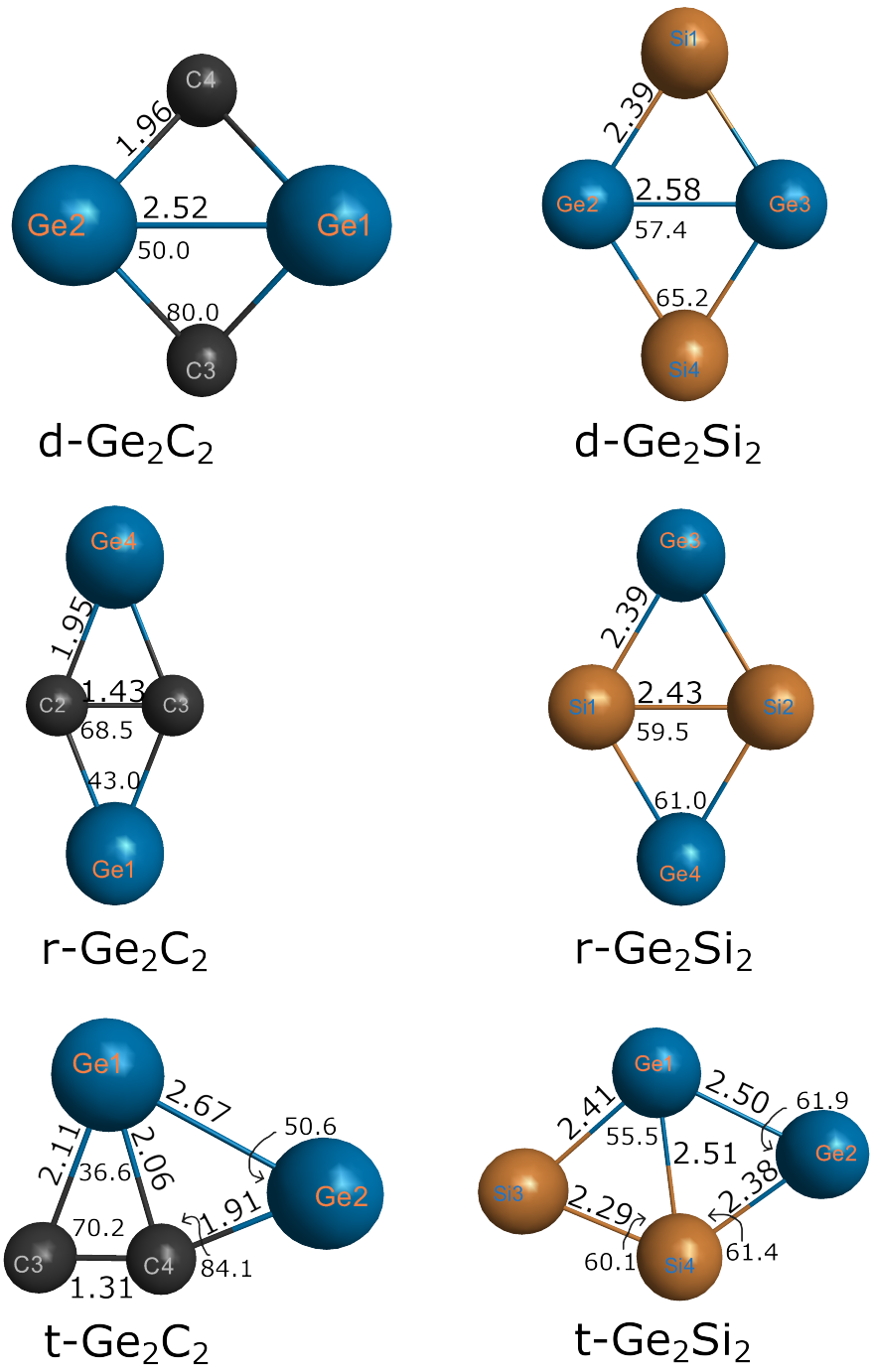

Figure 3: Optimized geometries of Ge_2Z_2 structures at the CCSD(T)-F12a/cc-pVTZ-F12 level of theory. Bond lengths shown in Å, angles in degrees. The d-Ge_2C_2 structure is in C_{2v} symmetry, with the carbon atoms going out of plane.

this structure likely shows some multi-reference character. To confirm the multi-reference character of the d-Ge_2C_2 structure, we carried out a CASSCF(16,16)/aug-cc-pVTZ[61–65] calculation at the CCSD(T)-F12a/cc-pVDZ-F12 optimized geometry to determine the configuration coefficients. The leading coefficient for the d-Ge_2C_2 structure is 0.8573, indicating large contributions from other configurations. To confirm single-reference character of the species, CASSCF single point calculations were carried out on each optimized structure and results are shown in Table S6. Notably, the leading coefficients in the expansion of the wavefunction for all other structures (not d-Ge_2C_2) were about 0.9. For the two Ge_3C structures which had T_1 values larger than 0.02, their CASSCF leading coefficients are still similar to those of the structures with smaller T_1 values. It may be worth re-examining these structures more thoroughly with multi-reference methods to see how the resulting structures and spectroscopic properties are affected.

Of the three Ge_2C_2 isomers, the t- structure has the lowest energy. The total energy of the r- structure is larger by 20 kJ mol^{-1}, and the d- isomer by 402 kJ mol^{-1}. The CASSCF single point calculations predict the same trends in energies, but predict a gap twice as large between the t- and d- structures at 800 kJ mol^{-1}. The CASSCF total and relative energies are shown in Table S6.

None of the vibrational modes for the t- isomer are relatively intense, however this molecule has a dipole moment of 3.52 D. The d- isomer has dipole moment of 2.52 D at the F12a/DZ level of theory, however, due to its multi-reference character it is uncertain whether this structure and dipole value are reliable. Lastly, the r- isomer of Ge_2C_2 has no net dipole moment, making only the t- isomer a likely candidate for detection by rotational spectroscopy.

Predicted vibrational frequencies for the Ge_2Si_2 isomers fall on the lower end of the detection range for JWST. Results for these three structures are shown in Tables S7 and S8. Each structure has only one vibrational mode that could be detected, with the r- isomer having the largest intensity for the ν_5 mode, the symmetric stretch of Ge(1)-Si(1) and Ge(1)-

Si(2) at 402.0 cm^{-1}, with an intensity of 119.8 km mol^{-1}. The isomer d-Ge_2Si_2 also has a relatively intense mode at 391.2 cm^{-1} with an intensity of 86.9 km mol^{-1}, however, it has larger energy by 32.637 kJ mol^{-1} than the isomer with the lowest energy, r-Ge_2Si_2.

Having D_{2h} symmetry, neither the r- nor d- isomer of Ge_2Si_2 exhibit dipole moments, and therefore could not be detected through rotational spectroscopy. Unlike the carbon analogue of the t- isomer, t-Ge_2Si_2 has a very small permanent dipole moment of 0.76 D, making it a less likely candidate for detection via rotational spectroscopy.

Table 6: Harmonic and anharmonic fundamental vibrational frequencies (in cm^{-1}) of Ge_2C_2 isomers at the F12a/TZ (and F12b/QZ, or F12a/DZ) level of theory. Intensities in km mol^{-1}.

Mode	Symmetry	Harmonic		Anharmonic		Intensity
r-Ge_2C_2		F12a/TZ	F12b/QZ	F12a/TZ	F12b/QZ	
6	A_g	1102.2	1103.2	1070.7	1071.8	0.0
5	B_{2g}	868.4	869.2	850.0	851.2	0.0
4	B_{1u}	816.1	816.9	801.7	802.7	307.2
3	A_g	281.9	282.3	271.9	272.0	0.0
2	B_{3u}	276.7	277.1	273.0	274.0	64.5
1	B_{2u}	147.3	147.2	147.1	147.6	11.9
MAPD				0.18		
t-Ge_2C_2		F12a/TZ				
6	A'	1581.2		1555.8		29.0
5	A'	575.8		570.2		45.8
4	A'	515.5		509.5		35.6
3	A'	392.5		391.0		11.0
2	A'	182.7		181.4		0.8
1	A''	179.1		178.7		3.8
d-Ge_2C_2		F12a/DZ				
6	A_1	599.7				0.0
5	B_1	550.7				0.0
4	B_2	444.4				0.0
3	A_2	415.0				0.0
2	A_1	280.9				0.0
1	A_1	233.1				0.0

Table 7: Equilibirum (e) and vibrationally-averaged (0) rotational constants of Ge_2C_2 isomers in MHz at the F12a/TZ level of theory and F12b/QZ level for r-Ge_2C_2. For r-Ge_2C_2, vibrationally-averaged rotational constants for its most intense mode, ν_4, are also included.

Constant	r-Ge_2C_2	F12b/QZ
A_e	41435.1	41476.6
B_e	1039.7	1040.3
C_e	1014.3	1014.8
A_0	41100.2	41140.1
B_0	1036.9	1037.5
C_0	1011.3	1011.8
A_4	41110.0	41149.5
B_4	1035.6	1036.2
C_4	1010.0	1010.6
MAPD		0.07
	t-Ge_2C_2	F12a/TZ
A_e		7721.4
B_e		1824.1
C_e		1475.5
A_0		7684.6
B_0		1822.3
C_0		1472.0
	d-Ge_2C_2	F12a/DZ
A_e		9435.3
B_e		2129.4
C_e		1770.7

Ge_3Z

The optimized Ge_3Z structures are shown in Figure 4. None of these four molecules show strong permanent dipole moments with the d- Ge_3C and Ge_3Si isomers having the largest at 0.98 D and 0.76 D, respectively. These molecules are thus more likely to be identified through their vibrational spectra. Results for the Ge_3C structures are shown in Tables 8 and 9, while vibrational frequencies for the Ge_3Si structures are collected in Table S9. Both r- isomers exhibit ν_6 vibrational modes at 941.8 cm^{-1} and 407.3 cm^{-1}, and with relatively large intensities of 103.2 km mol^{-1} and 81.1 km mol^{-1} for r-Ge_3C and r-Ge_3Si, respectively. Another predicted intense mode is the ν_5 mode of r-Ge_3C at 513.6 cm^{-1} with an intensity of 87.9 km mol^{-1}. The r- carbon structure lies 189.778 kJ mol^{-1} below the d- isomer (Table 1), making it more likely to be detected through its stronger IR spectra. The r- silicon isomer lies only 15.670 kJ mol^{-1} below the d- isomer, suggesting it may be possible to see interconversion between the two with such a small energy difference, assuming a small barrier between them. However, due to the r- isomer having a more intense vibrational mode in its spectrum, it is likely that the r- isomer would be detected over the d- isomer.

Table 8: Harmonic and anharmonic fundamental vibrational frequencies in cm^{-1} of Ge_3C isomers using F12a/TZ. Intensities in km mol^{-1}.

Mode	Symmetry	Harmonic	Anharmonic	Intensity
d-Ge_3C				
6	A′	626.0	619.2	6.8
5	A″	513.0	499.7	0.7
4	A′	271.6	271.1	0.4
3	A′	228.6	225.0	26.3
2	A″	151.0	150.0	0.1
1	A′	63.6	31.8	18.3
r-Ge_3C				
6	B_2	956.4	941.8	103.2
5	A_1	518.4	513.6	87.9
4	A_1	291.8	300.7	7.7
3	B_2	200.8	198.7	10.4
2	A_1	178.9	176.7	2.3
1	B_1	140.5	141.5	2.9

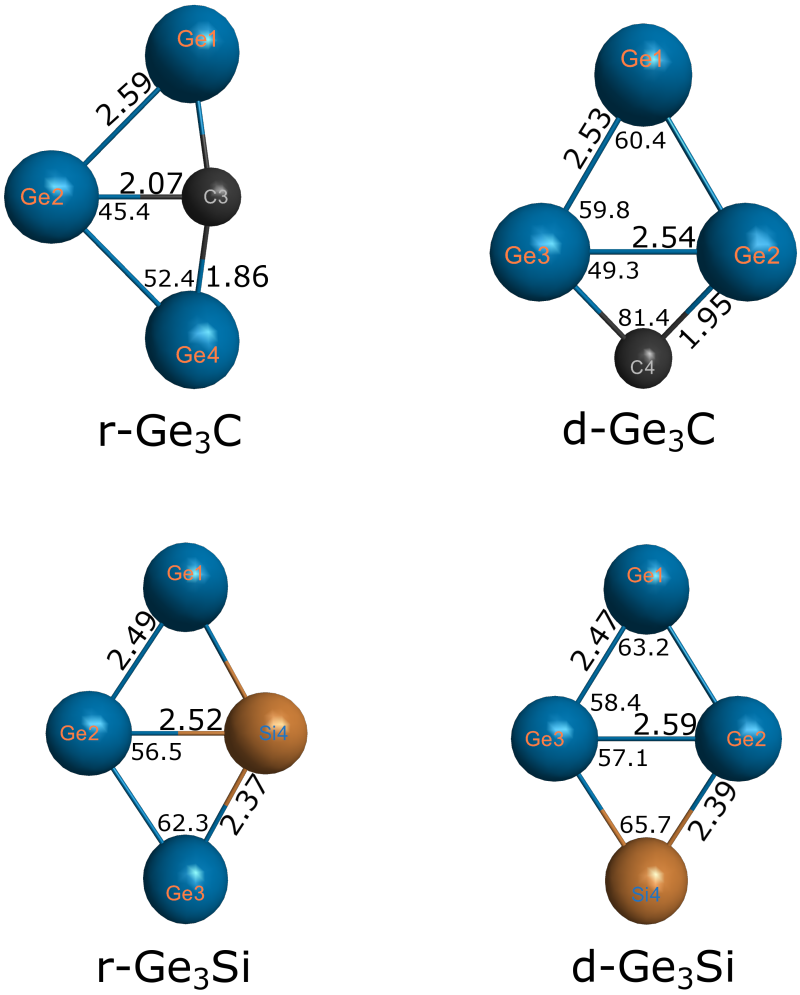

Figure 4: Optimized geometries of Ge_3Z structures at the CCSD(T)-F12a/cc-pVTZ-F12 level of theory. Bond lengths shown in Å, angles in degrees.

Table 9: Equilibirum (e) and vibrationally-averaged (0) rotational constants of Ge_3C and Ge_3Si isomers in MHz at the F12a/TZ level of theory. Vibrationally-averaged constants for most intense vibration for each isomer are also included.

Constant	d-Ge_3C	Constant	r-Ge_3C	Constant	d-Ge_3Si	r-Ge_3Si	
A_e	2108.1	A_e	2949.3	A_e	2031.9	A_e	3216.0
B_e	1746.3	B_e	1002.5	B_e	1259.3	B_e	789.8
C_e	959.8	C_e	748.2	C_e	777.5	C_e	634.0
A_0	2113.4	A_0	2937.6	A_0	2027.8	A_0	3207.8
B_0	1736.0	B_0	1001.5	B_0	1257.2	B_0	788.7
C_0	955.1	C_0	746.4	C_0	775.8	C_0	632.9
A_3	2107.6	A_6	2916.9	A_6	2019.8	A_6	3186.0
B_3	1737.4	B_6	1005.7	B_6	1258.5	B_6	790.2
C_3	954.5	C_6	748.4	C_6	777.0	C_6	634.3

Isotopic Substitution

Unlike carbon and silicon, germanium does not have a dominant, naturally occurring isotope. Instead, the majority of abundance is split between three isotopes: ^{74}Ge, ^{72}Ge, and ^{70}Ge, with abundances of 36.5%, 27.4%, and 20.5%, respectively.[43] The two other naturally occurring isotopes, ^{73}Ge and ^{76}Ge, have abundances of 7.76% and 7.75%, respectively.[43] As there is no singular dominant isotope of germanium, it is important to consider how isotopic substitution will affect the results of each structure studied herein.

Electronic energies will not change, and optimized structures will stay the same within 1x10^{-5} Å (due to numerical convergence thresholds), but frequencies, rotational constants, and zero-point energies will change. To show how they might change, results were also collected using the average isotopic mass of germanium as calculated by MOLPRO (72.59 amu). Anharmonic frequencies and intensities for r-GeC_3, r-Ge_2C_2, and r-Ge_3C are collected in Table 10 and compared with the results obtained used the mass of ^{74}Ge (73.92 amu). Frequencies using the average isotopic mass of germanium show a MAPD of 0.05%, 0.20%, and 0.54% for r-GeC_3, r-Ge_2C_2, and r-Ge_3C, respectively. Clearly, there is some deviation as the masses change, and that deviation will be larger as the masses are further changed

from ^{74}Ge, but the deviation will likely be quite small for each isotopic substitution. This will result in broader peaks in the IR spectra, but they will likely still be distinguishable for each species even with the inclusion of varying isotopes of germanium. The difference in frequencies and intensities between the two germanium masses (72.59 and 73.92 amu) is represented graphically in Figure 5.

One should also consider the likelihood of finding each species with each isotope present to know which combinations are the most likely to be observed. The probabilities of all unique combinations (320, excluding chemically equivalent duplicates) of the five germanium isotopes for each species considered in this work are collected in Tables S10-S13. For each species, those composed of entirely ^{74}Ge isotopes have the highest probability of being present, while substitutions with ^{72}Ge follow as next most likely.

Conclusions

This work presents anharmonic vibrational frequencies and rotational constants evaluated at a high-level of theory for a suite of tetra-atomic germanium carbide and silicide molecules. For many of these molecules, we report the only available computed frequencies and rotational constants, and for those that have already been studied, this work offers results from more accurate, recent methods. The spectroscopic data provide a reference for potential observation of the various species in the interstellar medium, specifically with instruments such as JWST through their IR spectra. Multiple structures have vibrational modes that are suitable for observation, the most promising of which is the ν_4 mode of r-Ge_2C_2 with a frequency of 802.7 cm^{-1} (12.5 μm) and an intensity of 307.2 km mol^{-1}. Other modes of potential interest include the ν_5 mode of r-Ge_2Si_2 at 402.0 cm^{-1} (24.9 μm) and 119.8 km mol^{-1}, the ν_6 mode of r-Ge_3C at 941.8 cm^{-1} (10.6 μm) and 103.2 km mol^{-1}, and the ν_6 modes of r-GeC_3 and r-$GeSi_3$ at 1538.3 cm^{-1} (6.5 μm) and 112.0 km mol^{-1} and 495.8 cm^{-1} (20.2 μm) and 107.0 km mol^{-1}, respectively. Some molecules also could be detected through

Table 10: Anharmonic vibrational frequencies (in cm^{-1}), intensities (in km mol^{-1}), and their relatives values when atomic mass of germanium is changed. Masses used are that of ^{74}Ge (73.92 amu), and the average atomic isotopic mass of germanium as calculated by MOLPRO (72.59 amu). MAPDs are shown for the values calculated with the average isotopic mass with respect to those calculated with the mass of ^{74}Ge.

Mode	Symmetry	m(Ge)=72.59		m(Ge)=73.92	
r-GeC_3		Anharm.	Int.	Anharm.	Int.
6	B_2	1537.5	111.9	1538.3	112.0
5	A_1	1096.0	2.2	1096.3	2.2
4	A_1	709.7	28.3	709.8	28.1
3	A_1	409.4	27.4	408.8	26.9
2	B_2	332.5	2.4	332.4	2.4
1	B_1	191.7	24.6	191.8	24.6
MAPD		0.05	0.44		
r-Ge_2C_2		Anharm.	Int.	Anharm.	Int.
6	A_g	1070.5	0.0	1070.7	0.0
5	B_{2g}	850.3	0.0	850.0	0.0
4	B_{1u}	802.5	307.7	801.7	307.2
3	A_g	273.1	0.0	271.9	0.0
2	B_{3u}	274.3	64.6	273.0	64.5
1	B_{2u}	147.3	12.0	147.1	11.9
MAPD		0.20	0.17		
r-Ge_3C		Anharm.	Int.	Anharm.	Int.
6	B_2	942.1	103.5	941.8	103.2
5	A_1	514.1	87.9	513.6	87.9
4	A_1	304.7	7.9	300.7	7.7
3	B_2	200.4	10.6	198.7	10.4
2	A_1	178.2	2.3	176.7	2.3
1	B_1	141.6	2.9	141.5	2.9
MAPD		0.54	0.80		

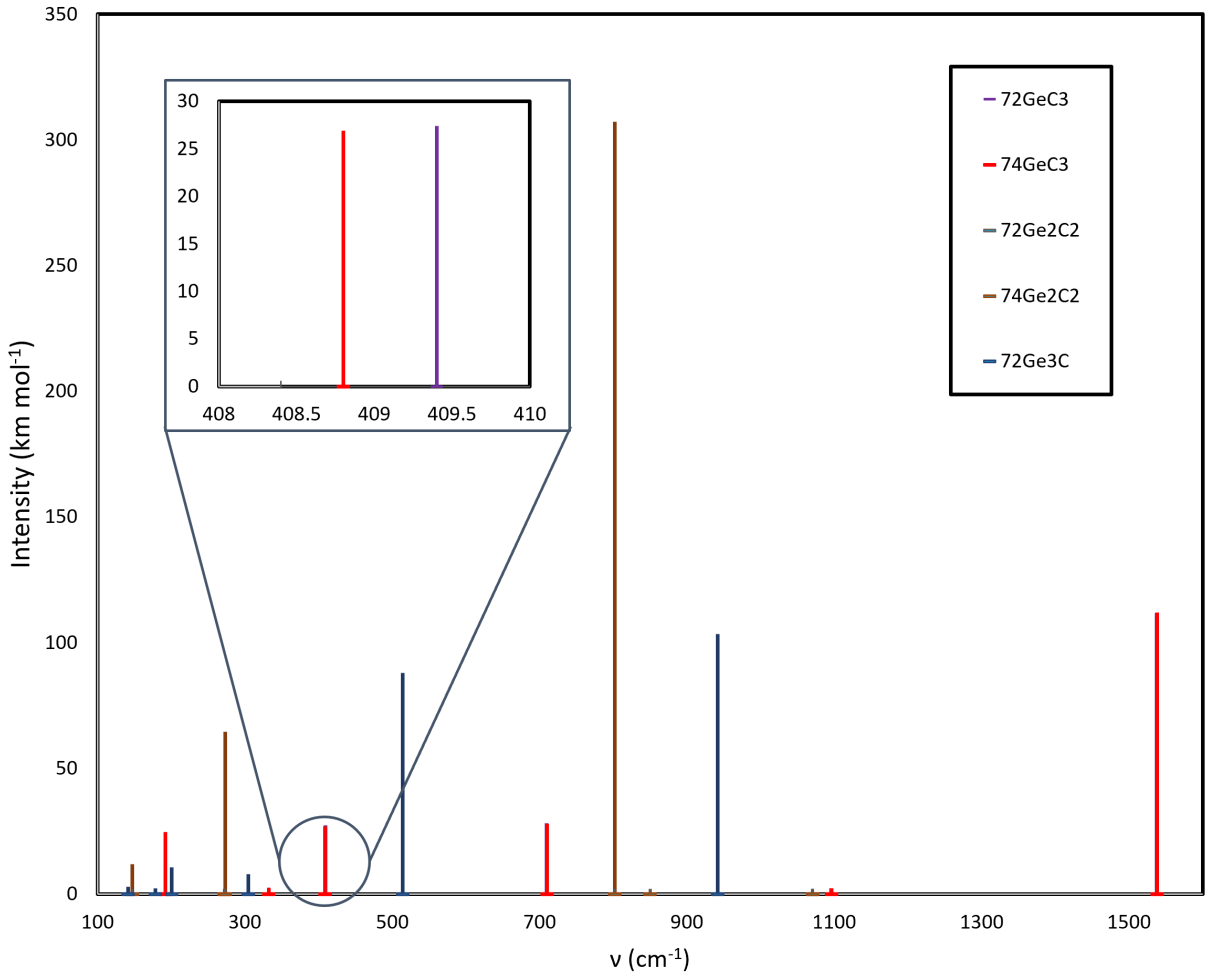

Figure 5: Theoretical IR spectra of r-GeC_3, r-Ge_2C_2, and r-Ge_3C computed using the mass of ^{74}Ge (73.92 amu) and the average isotopic mass (72.59 amu).

their rotational spectra due to their larger permanent dipole moments. These include d- and r-GeC_3 as well as t-Ge_2C_2 with net dipole moments of 5.40 D, 2.95 D and 3.52 D, respectively.

Many of the studied isomers have small energy differences, and it would be interesting to study the transition states between them to learn more about the internal conversion. The d-Ge_2C_2 structure, as well as some of the other species that show slight multi-reference character, also open up an interesting path for further computational study with accurate multi-reference approaches.

Due to germanium having isotopes with comparable, large abundances, it is important to consider the effect of different isotopes on the observed spectra. As the impact of isotopic substitution on vibrational frequencies is quite small, the result will be a slight broadening of the peaks in the IR spectrum, but the species should still be distinguishable. Combinations of isotopes containing primarily ^{74}Ge are most likely to be observed as ^{74}Ge is the most abundant isotope of the five naturally occurring isotopes.

With accurate spectroscopic data for these germanium-containing species, the presence of this heavier element in the interstellar can be studied more thoroughly, offering insight into the pathways it takes to end up in stars, proto-planetary systems and eventually other celestial bodies.

Acknowledgements

The authors thank the Digital Research Alliance of Canada (alliancecan.ca) for computing resources. A.B. & M.K. both thank the Natural Sciences and Engineering Research Council of Canada for the award of Discovery Grants.

Supporting Information Available

The relative zero-point vibrational energies of all species are including in the Supporting Information. Vibrational frequencies and/or rotational constants for r-C_4, r-Si_4, Ge_2Si_2 isomers, and Ge_3Si isomers are also collected in the SI. Probabilities of all possible combinations of germanium isotopes for each group of structures are available. Lastly, T_1 diagnostics, configuration coefficients from CASSCF computations, and Cartesian coordinates of all species studied are found in the SI.

References

(1) Osman, O.; Bekki, K.; Cortese, L. The role of dust destruction and dust growth in the evolution of the interstellar medium. *Mon. Not. R. Astron. Soc* **2020**, *497*, 2002–2017.

(2) Jørgensen, J. K.; Belloche, A.; Garrod, R. T. Astrochemistry During the Formation of Stars. *Annu. Rev. Astron. Astrophys.* **2020**, *58*, 727–778.

(3) Thaddeus, P.; Cummins, S. E.; Linke, R. A. Identification of the SiCC radical toward IRC +10216 : the first molecular ring in an astronomical source. *Astrophys. J. Lett.* **1984**, *283*, L45–L48.

(4) Bernatowicz, T.; Fraundorf, G.; Ming, T.; Anders, E.; Wopenka, B.; Zinner, E.; Fraundorf, P. Evidence for interstellar SiC in the Murray carbonaceous meteorite. *Nature* **1987**, *330*, 728–730.

(5) Cernicharo, J.; Gottlieb, C. A.; Guelin, M.; Thaddeus, P.; Vrtilek, J. M. Astronomical and Laboratory Detection of the SiC Radical. *Astrophys. J. Lett.* **1989**, *341*, L25.

(6) Mélinon, P.; Masenelli, B.; Tournus, F.; Perez, A. Playing with carbon and silicon at the nanoscale. *Nat. Mater.* **2007**, *6*, 479–490.

(7) Cernicharo, J. et al. Discovery of SiCSi in IRC+10216: A missing link between gas and dust carriers of Si–C bonds. *Astrophys. J. Lett.* **2015**, *806*, L3.

(8) Wooley, S.; Janka, T. The physics of core-collapse supernovae. *Nat. Phys* **2005**, *1*, 147.

(9) Sterling, N. C.; Dinerstein, H. L.; Bowers, C. W. Discovery of enhanced germanium abundances in planetary nebulae with the far ultraviolet spectroscopic explorer. *Astrophys. J.* **2002**, *578*, L55–L58.

(10) Burbidge, E. M.; Burbidge, G. R.; Fowler, W. A.; Hoyle, F. Synthesis of the elements in stars. *Rev. Mod. Phys.* **1957**, *29*, 547–650.

(11) Cowan, J. Astronomy: Elements of surprise. *Nature* **2003**, *423*, 29.

(12) Kunde, V.; Hanel, R.; Maguire, W.; Gautier, D.; Baluteau, J. P.; Marten, A.; Chedin, A.; Husson, N.; Scott, N. The tropospheric gas composition of Jupiter's north equatorial belt (NH_3, PH_3, CH_3D, GeH_4, H_2O) and the Jovian D/H isotopic ratio. *Astrophys. J.* **1982**, *263*, 443.

(13) Lam, K. W. F. et al. GJ 367b: A dense, ultrashort-period sub-Earth planet transiting a nearby red dwarf star. *Science* **2021**, *374*, 1271–1275.

(14) Apponi, A. J.; McCarthy, M. C.; Gottlieb, C. A.; Thaddeus, P. Astronomical Detection of Rhomboidal SiC_3. *Astrophys. J.* **1999**, *516*, L103.

(15) Prieto, L. V.; Cernicharo, J.; Quintana-Lacaci, G.; Agúndez, M.; Castro-Carrizo, A.; Fonfría, J. P.; Marcelino, N.; Zúñiga, J.; Requena, A.; Bastida, A.; Lique, F.; Guélin, M. Si-Bearing molecules toward IRC+10216: ALMA unveils the molecular envelope of CWLeo. *Astrophys. J. Lett.* **2015**, *805*, L13, https://europepmc.org/articles/pmc4681092?pdf=render.

(16) Sehring, C. M.; Palmer, C. Z.; Westbrook, B. R.; Fortenberry, R. C. The spectral features and detectability of small, cyclic silicon carbide clusters. *Front. Astron. Space Sci.* **2022**, *9*, 1074879.

(17) Apponi, A. J.; McCarthy, M. C.; Gottlieb, C. A.; Thaddeus, P. The rotational spectrum of rhomboidal SiC_3. *J. Chem. Phys.* **1999**, *111*, 3911–3918.

(18) McCarthy, M. C.; Apponi, A. J.; Thaddeus, P. A second rhomboidal isomer of SiC_3. *J. Chem. Phys.* **1999**, *111*, 7175–7178.

(19) McCarthy, M. C.; Gottlieb, C. A.; Cernicharo, J. Building blocks of dust: A coordinated laboratory and astronomical study of the archtype AGB carbon star IRC+10216. *J. Mol. Spectrosc.* **2019**, *356*, 7–20.

(20) Presilla-Márquez, J. D.; Graham, W. R. M. Vibrational spectra of tetra-atomic silicon–carbon clusters. I. Rhomboidal Si_3C in Ar at 10 K. *J. Chem. Phys.* **1992**, *96*, 6509–6514.

(21) Lammertsma, K.; Guner, O. F. Structures and energies of disilicon dicarbide, C_2Si_2. *J. Am. Chem. Soc.* **1988**, *110*, 5239–5245.

(22) Rittby, C. M. L. An abinitio study of the structure and infrared spectrum of Si_3C. *J. Chem. Phys.* **1992**, *96*, 6768–6772.

(23) Truong, N. X.; Savoca, M.; Harding, D. J.; Fielicke, A.; Dopfer, O. Vibrational spectra and structures of Si_nC clusters (n = 3–8). *Phys. Chem. Chem. Phys.* **2015**, *17*, 18961–18970.

(24) Savoca, M.; Langer, J.; Harding, D. J.; Dopfer, O.; Fielicke, A. Incipient chemical bond formation of Xe to a cationic silicon cluster: Vibrational spectroscopy and structure of the Si_4Xe^+ complex. *Chem. Phys. Lett.* **2013**, *557*, 49–52.

(25) Stanton, J. F.; Dudek, J.; Theulé, P.; Gupta, H.; McCarthy, M. C.; Thaddeus, P. Laser spectroscopy of Si_3C. *J. Chem. Phys.* **2005**, *122*, 124314.

(26) Presilla-Márquez, J. D.; Gay, S. C.; Rittby, C. M. L.; Graham, W. R. M. Vibrational spectra of tetra-atomic silicon–carbon clusters. II. Si_2C_2 in Ar at 10 K. *J. Chem. Phys.* **1995**, *102*, 6354–6361.

(27) Yadav, P.; Yadav, R.; Agrawal, S.; Agrawal, B. Theoretical study of the physical properties of binary Si_mC_n (m+n $\leq$ 5) clusters: An ab initio study. *Physica E Low Dimens. Syst. Nanostruct.* **2006**, *33*, 249–262.

(28) Wielgus, P.; Roszak, S.; Majumdar, D.; Leszczynski, J. Thermodynamic properties of germanium/carbon microclusters. *J. Chem. Phys.* **2005**, *123*, 234309.

(29) Wielgus, P.; Roszak, S.; Majumdar, D.; Saloni, J.; Leszczynski, J. Theoretical studies on the bonding and thermodynamic properties of GeSi clusters: The precursors of germanium/silicon nanomaterials. *J. Chem. Phys.* **2008**, *128*, 144305.

(30) Goswami, S.; Saha, S.; Yadav, R. Structural, electronic and vibrational properties of Ge_xC_y (x+y=2–5) nanoclusters: A B3LYP-DFT study. *Physica E Low Dimens. Syst. Nanostruct.* **2015**, *74*, 175–192.

(31) Zingsheim, O.; Martin-Drumel, M.-A.; Thorwirth, S.; Schlemmer, S.; Gottlieb, C. A.; Gauss, J.; McCarthy, M. C. Germanium Dicarbide: Evidence for a T-Shaped Ground State Structure. *J. Phys. Chem. Lett.* **2017**, *8*, 3776–3781.

(32) Koput, J. Ab initio potential energy surface and vibration–rotation energy levels of germanium dicarbide, GeC_2. *J. Comput. Chem.* **2018**, *39*, 1327–1334.

(33) Martin-Drumel, M.-A.; Baraban, J. H.; Changala, P. B.; Stanton, J. F.; McCarthy, M. C. The Hunt for Elusive Molecules: Insights from Joint Theoretical and Experimental Investigations. *Chem. Eur. J.* **2019**, *25*, 7243–7258.

(34) Lee, K. L. K.; Thorwirth, S.; Martin-Drumel, M.-A.; McCarthy, M. C. Generation and structural characterization of Ge carbides GeC_n (n = 4, 5, 6) by laser ablation, broadband rotational spectroscopy, and quantum chemistry. *Phys. Chem. Chem. Phys.* **2019**, *21*, 18911–18919.

(35) Hill, J. G.; Peterson, K. A. Correlation consistent basis sets for explicitly correlated wavefunctions: valence and core–valence basis sets for Li, Be, Na, and Mg. *Phys. Chem. Chem. Phys.* **2010**, *12*, 10460–10468.

(36) Watrous, A. G.; Westbrook, B. R.; Fortenberry, R. C. F12-TZ-cCR: A Methodology for Faster and Still Highly Accurate Quartic Force Fields. *J. Phys. Chem. A* **2021**, *125*, 10532–10540.

(37) Wang, X.; Huang, X.; Bowman, J. M.; Lee, T. J. Anharmonic rovibrational calculations of singlet cyclic C_4 using a new ab initio potential and a quartic force field. *J. Chem. Phys.* **2013**, *139*, 224302.

(38) Algranati, M.; Feldman, H.; Kella, D.; Malkin, E.; Miklazky, E.; Naaman, R.; Vager, Z.; Zajfman, J. The structure of C_4 as studied by the Coulomb explosion method. *J. Chem. Phys.* **1989**, *90*, 4617–4618.

(39) Blanksby, S. J.; Schröder, D.; Dua, S.; Bowie, J. H.; Schwarz, H. Conversion of Linear to Rhombic C_4 in the Gas Phase: A Joint Experimental and Theoretical Study. *J. Am. Chem. Soc.* **2000**, *122*, 7105–7113.

(40) Becke, A. D. Density-functional thermochemistry. III. The role of exact exchange. *J. Chem. Phys.* **1993**, *98*, 5648–5652.

(41) Lee, C.; Yang, W.; Parr, R. G. Development of the Colle-Salvetti correlation-energy formula into a functional of the electron density. *Phys. Rev. B* **1988**, *37*, 785–789.

(42) Hampel, C.; Peterson, K. A.; Werner, H.-J. A comparison of the efficiency and accuracy of the quadratic configuration interaction (QCISD), coupled cluster (CCSD), and Brueckner coupled cluster (BCCD) methods. *Chem. Phys. Lett.* **1992**, *190*, 1–12.

(43) Kondev, F.; Wang, M.; Huang, W.; Naimi, S.; Audi, G. The NUBASE2020 evaluation of nuclear physics properties. *Chin. Phys. C* **2021**, *45*, 030001.

(44) Raghavachari, K.; Trucks, G. W.; Pople, J. A.; Head-Gordon, M. A fifth-order perturbation comparison of electron correlation theories. *Chem. Phys. Lett.* **1989**, *157*, 479–483.

(45) Adler, T. B.; Knizia, G.; Werner, H.-J. A simple and efficient CCSD(T)-F12 approximation. *J. Chem. Phys.* **2007**, *127*, 221106.

(46) Knizia, G.; Adler, T. B.; Werner, H.-J. Simplified CCSD(T)-F12 methods: Theory and benchmarks. *J. Chem. Phys.* **2009**, *130*, 054104.

(47) Peterson, K. A.; Adler, T. B.; Werner, H.-J. Systematically convergent basis sets for explicitly correlated wavefunctions: The atoms H, He, B–Ne, and Al–Ar. *J. Chem. Phys.* **2008**, *128*, 084102.

(48) Hill, J. G.; Peterson, K. A. Correlation consistent basis sets for explicitly correlated wavefunctions: Pseudopotential-based basis sets for the post-d main group elements Ga–Rn. *J. Chem. Phys.* **2014**, *141*, 094106.

(49) Feller, D.; Peterson, K. A.; Hill, J. G. Calibration study of the CCSD(T)-F12a/b methods for C_2 and small hydrocarbons. *J. Chem. Phys.* **2010**, *133*, 184102.

(50) Werner, H.-J.; Knowles, P. J.; Knizia, G.; Manby, F. R.; Schütz, M. Molpro: a general-purpose quantum chemistry program package. *Wiley Interdiscip. Rev. Comput. Mol. Sci.* **2012**, *2*, 242–253.

(51) Werner, H.-J. et al. The Molpro quantum chemistry package. *J. Chem. Phys.* **2020**, *152*, 144107.

(52) Werner, H.-J. et al. MOLPRO, 2023.2, a package of ab initio programs. See https://www.molpro.net.

(53) Eckert, F.; Pulay, P.; Werner, H.-J. *Ab Initio* Geometry Optimization for Large Molecules. *J. Comput. Chem.,* **1997**, *18*, 1473.

(54) Rauhut, G.; El Azhary, A.; Eckert, F.; Schumann, U.; Werner, H.-J. Impact of Local Approximations on MP2 Vibrational Frequencies. *Spectrochim. Acta A* **1999**, *55*, 651.

(55) Hrenar, T.; Rauhut, G.; Werner, H.-J. Impact of Local and Density Fitting Approximations on Harmonic Vibrational Frequencies. *J. Phys. Chem. A,* **2006**, *110*, 2060.

(56) Ziegler, B.; Rauhut, G. Efficient generation of sum-of-products representations of high-dimensional potential energy surfaces based on multimode expansions. *J. Chem. Phys.* **2016**, *144*, 114114.

(57) Rauhut, G. Efficient calculation of potential energy surfaces for the generation of vibrational wave functions. *J. Chem. Phys.* **2004**, *121*, 9313–9322.

(58) Ramakrishnan, R.; Rauhut, G. Semi-quartic force fields retrieved from multi-mode expansions: Accuracy, scaling behavior, and approximations. *J. Chem. Phys.* **2015**, *142*, 154118.

(59) Ziegler, B.; Rauhut, G. Rigorous use of symmetry within the construction of multidimensional potential energy surfaces. *J. Chem. Phys.* **2018**, *149*, 164110.

(60) Lee, T. J.; Taylor, P. R. A diagnostic for determining the quality of single-reference electron correlation methods. *Int. J. Quantum Chem.* **1989**, *36*, 199–207.

(61) Roos, B. O.; Taylor, P. R.; Sigbahn, P. E. A complete active space SCF method (CASSCF) using a density matrix formulated super-CI approach. *Chem. Phys.* **1980**, *48*, 157–173.

(62) Werner, H.; Knowles, P. J. A second order multiconfiguration SCF procedure with optimum convergence. *J. Chem. Phys.* **1985**, *82*, 5053–5063.

(63) Roos, B. O. The Complete Active Space Self-Consistent Field Method and its Applications in Electronic Structure Calculations. *Adv. Chem. Phys.* **1987**, *69*, 399–445.

(64) Kendall, R. A.; Dunning, J., Thom H.; Harrison, R. J. Electron affinities of the first-row atoms revisited. Systematic basis sets and wave functions. *J. Chem. Phys.* **1992**, *96*, 6796–6806.

(65) Kreplin, D. A.; Knowles, P. J.; Werner, H.-J. Second-order MCSCF optimization revisited. I. Improved algorithms for fast and robust second-order CASSCF convergence. *J. Chem. Phys.* **2019**, *150*, 194106.